Efficient Macromodeling of Defect Propagation/Growth Mechanisms in VLSI Fabrication

Xiaolei Li, Andrzej J. Strojwas, *Fellow, IEEE,* Mahesh Reddy, and Linda S. Milor, *Member, IEEE*

***Abstract*— Particulate contamination deposited on silicon wafers is typically the dominant reason for yield loss in VLSI manufacturing. The transformation of contaminating particles into defects and then electrical faults is a very complex process which depends on the defect location, size, material, and the underlying IC topography. An efficient defect macromodeling methodology based on the rigorous two-dimensional (2-D) topography simulator METROPOLE, has been developed to allow the prediction and correlation of the critical physical parameters (material, size, and location) of contamination in the manufacturing process to device defects. The results for a large number of defect samples simulated using the above approach were compared with the data gathered from the AMD-Sunnyvale fabline. A good match was obtained indicating the accuracy for our method of developing contamination to defect propagation/growth macromodels.**

***Index Terms*— Defect particle, semiconductor fabrication, topography modeling.**

I. Introduction

MODERN VLSI manufacturing technologies consist of a large number of complex and expensive process steps. Contamination resulting in possible yield loss can be introduced at any of these steps. In-line inspection detects the defects in various process steps and yield improvement is then performed through the identification and subsequent elimination of the defect sources. It has been seen that defects may grow in size from one process step to the next and as a result cause faults in a later process step. In order to distribute the defect inspection resources in the most efficient way, we need to determine the yield impact of the defects including the propagation/growth effects. This will allow the determination of the sampling plan at each process level and the choice of the most appropriate inspection sensitivity (pixel size) to capture the killer defects [1].

Contamination in the fabrication process may be in the form of particles of various sizes and composition that may be located in various positions on the wafer structures. The contamination is usually in the form of unwanted particles or liquid droplets deposited on the wafer during fabrication steps. After deposition, lithography and etching steps, an extra pattern or absence of a pattern may occur. These deviations from the intended wafer patterns produce defects. For example, one spot defect may cause a short, while another one may result in a break.

It has been seen that defects may propagate and grow throughout the process flow, and as a result cause faults in the final product. In recent studies, it was found that there are two major defect propagation mechanisms, namely inter-layer and intra-layer defect propagations. Inter-layer propagation refers to the defects that propagate and grow in size from one layer to the next (e.g., from poly to metal1). With the introduction of CMP into the process flow, the inter-layer defect propagation between back-end process layers was greatly reduced. However, as we will show later in this paper, there is still a significant defect propagation among front-end layers. By intra-layer propagation, we mean defects that propagate and grow in size from one process step to next within a given layer (e.g., metal1). For example, a metal defect that propagates and grows through deposition, lithography and etch steps represents an intra-layer propagation. Thus, in addition to in-line defect inspection and other physical characterization methods (SEM, EDS etc.), modeling is needed to capture the defect propagation and growth, perform early diagnosis of killer defects and accurately predict yield.

In order to characterize the effects of particle size, location and composition on the formation of defects following deposition, photoresist exposure, development and etching, the physical nature of the contamination to defect transformation should be studied. The relationship between contamination particles and defects after lithography, etching and deposition steps may be effectively simulated using our two-dimensional (2-D) topography simulator METROPOLE [3], [4].

Physically based simulators such as METROPOLE are, however, too expensive and computationally prohibitive to predict yield impact. We have developed a methodology to study the defect transformation and propagation phenomenon, which will be described in the next section. The strength

Manuscript received December 30, 1997; revised March 27, 1998. This work was supported by the Semiconductor Research Corporation, Pennsylvania Sematech Center of Excellence for Rapid Yield Learning under Contract MC-511, AMD-Sunnyvale, and PDF Solutions, Inc.

X. Li was with the Department of Electrical and Computer Engineering, Carnegie Mellon University, Pittsburgh, PA 15213 USA. He is now with PDF Solutions, Inc., San Jose, CA 95110 USA (e-mail: xili@pdf.com).

A. Strojwas is with the Department of Electrical and Computer Engineering, Carnegie Mellon University, Pittsburgh, PA 15213 USA.

M. Reddy was with the Department of Electrical and Computer Engineering, Carnegie Mellon University, Pittsburgh, PA 15213 USA. He is now with the KLA-Tencor, Inc., Richardson, TX 75081 USA (e-mail: Mahesh.Reddy@kla-tencor.com).

L. Milor is with the Advanced Micro Devices, Inc., Sunnyvale, CA 94088 USA.

Publisher Item Identifier S 0894-6507(98)08371-7.

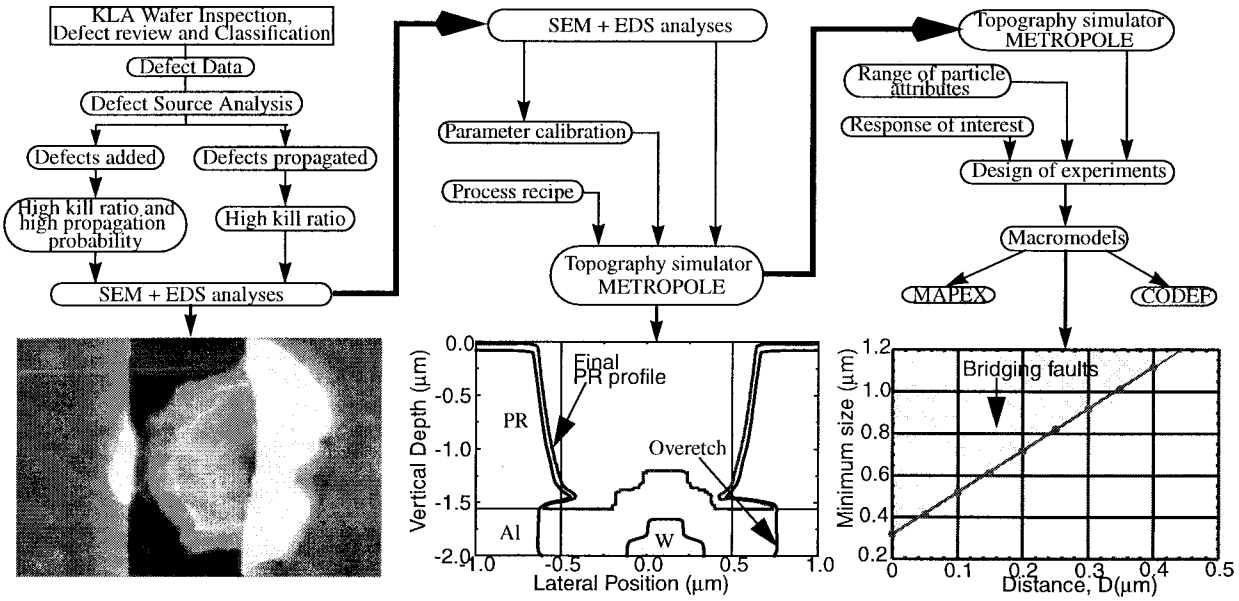

Fig. 1. Macromodel development methodology.

of this simulation-based defect analysis approach is that the simulators can be fine-tuned with a small set of carefully designed experiments. A more comprehensive set of simulation experiments can then be run to provide a sufficient amount of data to build the macromodels relating the final defect characteristics to the original contamination particle attributes such as location (with respect to the surrounding features, nonplanarities, etc.), size (physical dimension) and chemical composition.

The emphasis of this paper is on the development of a defect macromodeling methodology in IC fabrication. We introduce our new methodology for defect propagation/growth macromodeling based on rigorous topography simulation in Section II. Then, we present our experimental and modeling results in Section III, followed by a summary in Section IV.

II. Defect Modeling Methodology

In this section, a methodology for studying the yield impact of critical yield limiting defects that propagate through process steps is presented. This methodology combines the physical measurements and analyzes of in-line defects, intensive simulations and the extraction of simulation results in the form of macromodels [5]. This methodology can be applicable to different devices and processes. The flow chart of the macromodeling development methodology is shown in Fig. 1.

We start with the in-line defect inspection (e.g., by KLA-Tencor machines) of the same wafers at each inspection step. Defects captured by the inspection tool are classified into different types using the inspection system or other off-line review stations. An analysis is conducted on the classified defects by type to obtain an estimate of kill ratio (impact on yield) and the probability of propagation. The KLA 255X station provides an analysis mode, called DSA (defect source analysis) which allows defects to be separated into adders (defects that are detected for the first time at a particular inspection step) and commons (defects that propagate from previous processing layers). Common defects with a high estimated kill ratio, and adder defects with a combination of a high estimated kill ratio and probability of propagating to later levels are chosen. For each selected defect, top-view and tilted SEM (scanning electron microscope) analyzes are performed to obtain detailed physical properties of the defect (e.g., precise location, size, etc.). The SEM's we used have very accurate stage positioning system, so that we can locate defect at center of the viewing window. The addition of an EDS (energy dispersion spectroscopy) system to the SEM provides convenient elemental analysis of contaminants. Defects that propagate are again tagged at later levels and reviewed on the SEM/EDS for a change in size due to the "decoration" effect. The SEM/EDS review stations, in combination with automated defect detection tools, provide a powerful closed-loop analysis system and allow for the detailed study of defects that propagate from one level to the next.

After the defect data collection, the next procedure involves the simulation of defect transfer by the general-purpose topography simulator METROPOLE, which is capable of simulating nonplanar substrate accurately and efficiently. In the defect study, this simulator allows defects to be simulated at a particular process step or between different process steps as the defect propagates from one level to the next. In order to accomplish this, it is necessary to have a good understanding of the process flow and recreate cross-sections of the structures from the SEM in the ideal case without the defect and in the actual case with the defect. The process recipe with the layer stacking is a required input to the simulator. Parameters such as the refractive indices of materials, deposition, and etch times are tuned to model the structure to obtain an ideal profile with no defect. Using the same parameters as in the ideal case, the scenario with the defect is simulated next to obtain a match with the defect SEM's.

The next step is the most time-consuming and involves designing appropriate simulation experiments to extract the

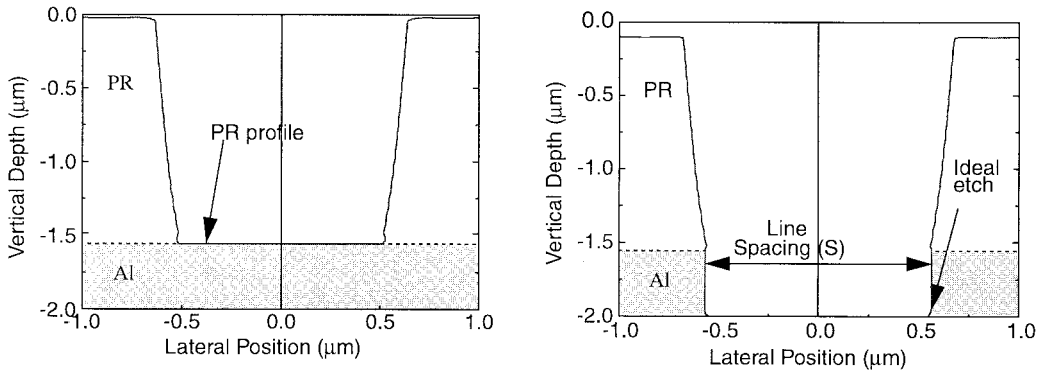

Fig. 2. (a) Simulation of ideal case after PR exposure and development and (b) simulation profile after Al etching.

macromodels. These simulation experiments involve changing physical characteristics such as size (height and width), chemical composition and location of the particle. Physical characteristics are varied, mostly one or two at a time, as the relationships are otherwise too complex to model and explain physically. Suitable ranges for the particle attributes have to be selected. This is done after evaluating the effects (whether a particle causes bridging faults, opens, electromigration hazards, etc.) of numerous particles with different attributes. Finally, the response of interest (e.g., line-edge shift, minimum size of a defect that causes a fault, region in space where bridging occurs, etc.) is chosen depending on the effects of the particle. For instance, following deposition, particles are found to grow in lateral direction (diameter) and an appropriate response is the increase in the particle width. Another example of a response is the line spacing as the particle location changes. Once the range and the response of interest are determined, the simulation experiment is designed and run. It should be noted that an important assumption was made during the simulation process: the top resist surface is still flat despite the presence of defect underneath, thus we ignore resist thickening effect.

The last step involves extracting the results from the simulation experiments in the form of appropriate macromodels. These macromodels for the response of interest are expressed as a function of the physical characteristics of the particle. In some other cases, the complexity of the macromodel makes it impossible to express the response of interest as a single function over an entire range. In such cases, the range is split into smaller intervals and functions are derived over these smaller intervals in a much simpler manner. The macromodels developed can be then fed to the yield prediction tools, such as MAPEX [9], or tools that simulate the transformation of contamination from one processing level to the next, such as CODEF [10]. The general methodology outlined here was employed in several studies, each of which is discussed in the next section.

III. Modeling and Experimental Results

A. Tungsten Defect Study

To illustrate our approach, we consider here a simple metal line structure. On the top of an insulating layer, an aluminum layer and a TiN antireflective coating (ARC) were deposited. The structure was covered by a layer of photoresist and exposed with randomly polarized i-line illumination. Subsequent photoresist development produced a given line spacing, S, of 1.1 μm. Fig. 2 shows the resulting structure after photoresist development and after aluminum was etched to the insulating substrate. If a tungsten particle is present in the material structure, the light distribution pattern within the photoresist is distorted. Fig. 3 shows the vertical cross-section of the light intensity distribution within the PR during the exposure if a metal defect is present in the middle of line spacing. Because of the scattering effect of the metal particle, an erroneous light intensity pattern was observed. It should be noted that the light intensity distribution could not be measured experimentally, so the rigorous simulation provides the physical insight to the interaction between the contamination particle and incident light beam.

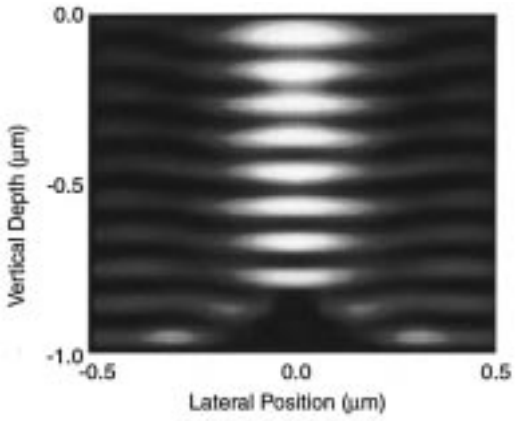

Fig. 3. Light intensity within PR in the presence of W defect.

The photoresist profile after exposure and development was distorted, as seen in Fig. 4(a). The original elliptical particle of width 0.35 μm (vertical height is 0.3 μm) is seen to grow in the lateral direction to about 0.6 μm after the aluminum deposition. Fig. 4(b) illustrates how the distorted photoresist profile can result in a bridging fault after the nominal aluminum etch process if there is a tungsten particle underneath the aluminum line. Simulation results also indicate that a particle of size 0.35 μm after deposition would not result

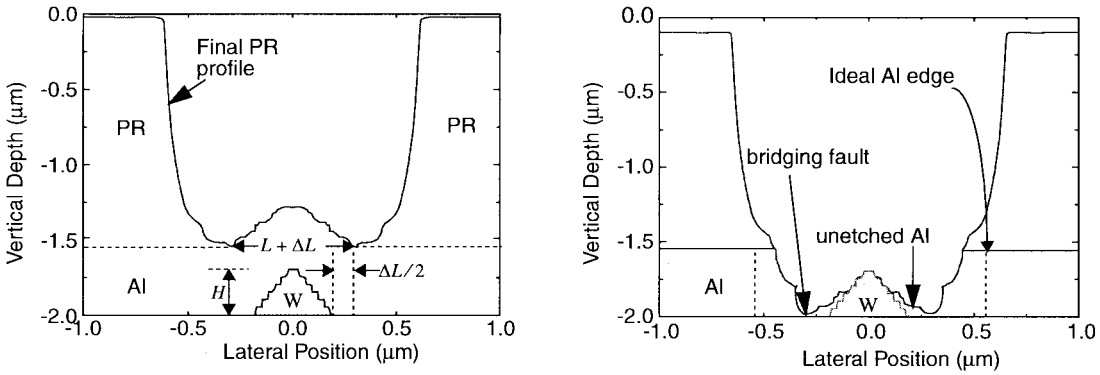

(a) (b)

Fig. 4. (a) Simulation of the tungsten defect after PR exposure and development and (b) simulation profile of tungsten defect after Al etching, a bridging fault was caused by the W defect.

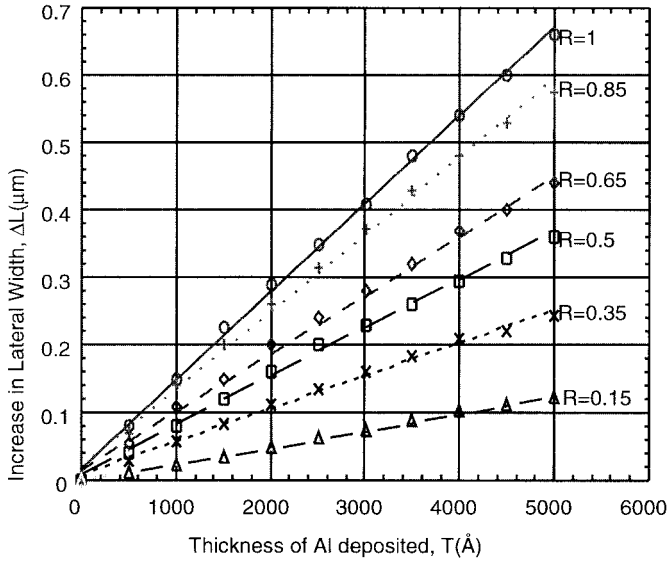

Fig. 5. Graph of ΔL versus T for different ratios, R.

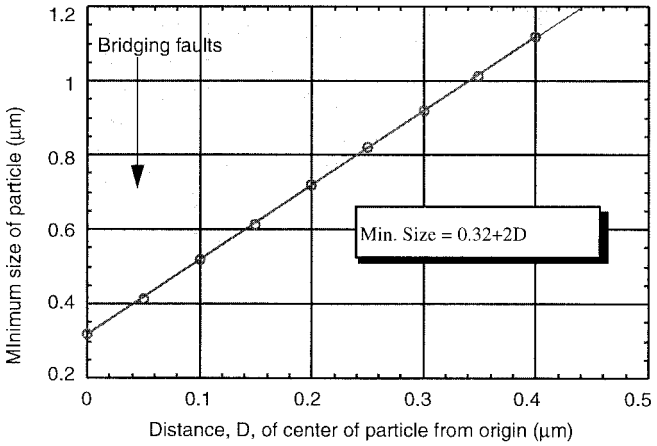

Fig. 6. Graph of minimum size of particle that causes fault versus distance of particle from center.

in a fault (not shown here). A combination of the lateral growth of the defect during the deposition and the photolithographic effect of the photoresist not being developed as in the ideal case results in the bridging fault.

A relationship between the lateral growth of the defect and the thickness of the deposited aluminum was investigated through numerous simulations. In the deposition simulation module of METROPOLE, a parameter R, which is the ratio of *isotropic deposition rate to total deposition rate*, is used within string-like surface advancement algorithms. In these simulations, the total deposition rate was kept constant and different values for R between 0 and 1 were chosen. A graph of lateral width increase, ΔL versus thickness of aluminum deposited, T was plotted for each of these ratios, as seen in Fig. 5. For each ratio R there exists a linear relationship between the increase in the lateral width of the defect and the thickness of aluminum deposited. Furthermore, for a given thickness of aluminum deposited, ΔL increases as R increases.

The effects of particle location on defect and fault formation were also studied in this case. The minimum width of tungsten particles that result in faults was determined through simulations. With all the process parameters held constant, and at a ratio (R) of 0.5, we observed that as the center of the particle is moved away from the origin (symmetric with respect to the mask) the width of the original tungsten particle has to be larger in order to cause a fault. This can be seen in Fig. 6. For a bridging fault to occur, the following relation must hold:

$$L_{\min} > 0.32 + 2D \tag{1}$$

where D is distance between the center of the particle and the center of line space (origin) and $L_{\min}$ is the minimum particle size to cause a fault at any location.

In general, the minimum particle size that causes a fault at any location should be greater than the sum of the minimum particle size that causes a fault at the origin ($L^0_{\min}$) and twice the distance of the particle from the origin,

$$L_{\min} > L^0_{\min} + 2D. \tag{2}$$

Fig. 7 shows a tungsten particle with a different vertical size. Instead of a bridging fault, it only generates narrowing of the aluminum lines and increases the possibility of electromigration during circuit operation. Fig. 8 shows experimental results of the defect analysis conducted at the AMD Sunnyvale fab. A good match was obtained between the simulation (Fig. 7)

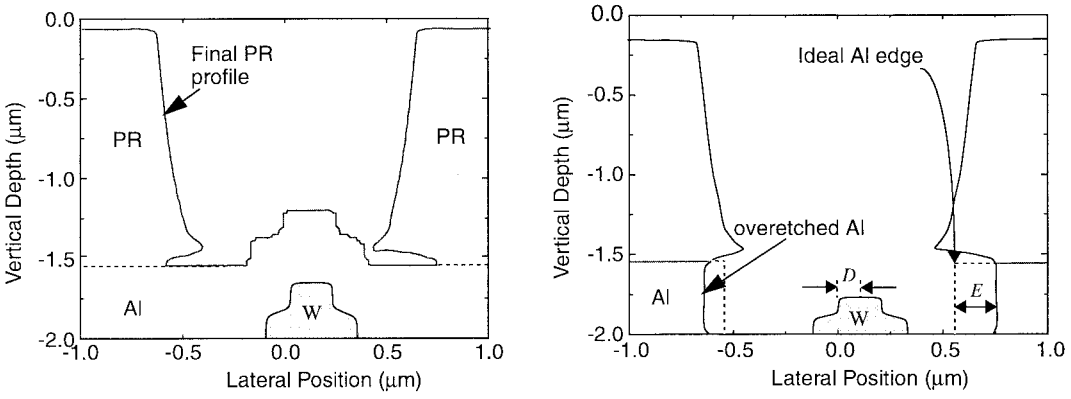

Fig. 7. (a) Simulation of the tungsten defect after PR exposure and development and (b) simulation profile of tungsten defect after Al etching, overetching was caused by W defect.

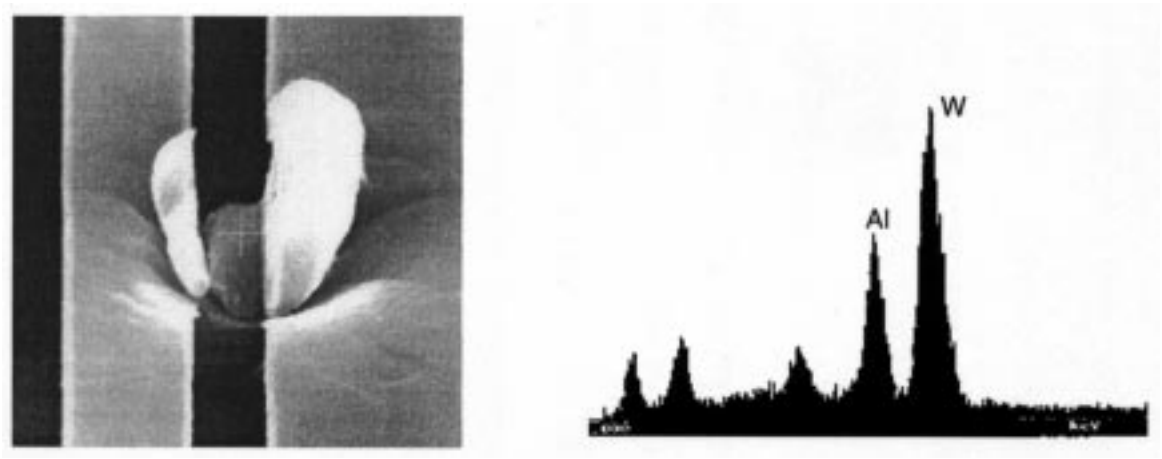

Fig. 8. (a) The SEM picture of a particle embedded in the Al layer and (b) an EDS study indicates the particle is a tungsten particle.

and experimental results (Fig. 8). As the vertical height of the particle increases from 0.3 to 0.35 μm, the line-edge shift turns negative. These positive and negative line-edge shifts are shown in Figs. 4 and 7, respectively. The effects of these line-edge shifts are also different, with the 0.3-μm particle causing bridging faults and the 0.35-μm particle resulting in electromigration hazards. This difference is caused by the different scattering patterns of the underlying defects. If the height of defect is high, the slope of the defect sidewall is steep, then more light is scattered toward the side of the defect. Thus over-etching and electromigration is present in the process. On the other hand, if defect sidewall is gradual, then more light will be scattered back up to the top of defect, thus cause underdevelopment and bridging fault.

The line-edge shift E after photoresist exposure and development was investigated with respect to different heights H and widths L of the tungsten particle following deposition of aluminum. In this study, the particle was assumed to be centered, i.e., symmetric with respect to the mask. This relationship is shown in Fig. 9. For heights less than 0.2 μm, the line-edge shift is virtually negligible. For heights greater than 0.2 μm, the width of the particle is dominant in determining the extent of the shift (wider particles exhibited increased shifts) and the height determines the direction of shift (positive or negative). Following aluminum etch, line-edge shifts greater than 0.15 μm result in bridging faults while the line-edge shifts less than -0.45 μm result in open circuits. Electromigration is considered to be a risk for line shifts in the range of -0.20 to -0.45 μm. The line-edge shift E was modeled as a function of the particle height and width and is given by (3) for $0.1\,\mu\text{m} < L < 0.5$ μm and $H > 0.2$ μm:

$$E = (-0.98 - 2.21L) + (7.96 + 17.46L)H + (-18.95 - 28.40L)H^2. \quad (3)$$

Each curve in Fig. 9 was initially modeled by a quadratic equation with height being the independent variable. Equation (3) was obtained by relating the coefficients of the quadratic to the width of the particle.

Thus far, the tungsten particle was always considered to be positioned symmetrically with respect to the mask opening. For the tungsten particle of width 0.3 μm and height 0.3 μm at different locations, the relationship between the total line spacing S versus the distance D of the center of the particle from the origin (origin is symmetrical with respect to the mask) is shown in Fig. 10. The only location where a bridging fault

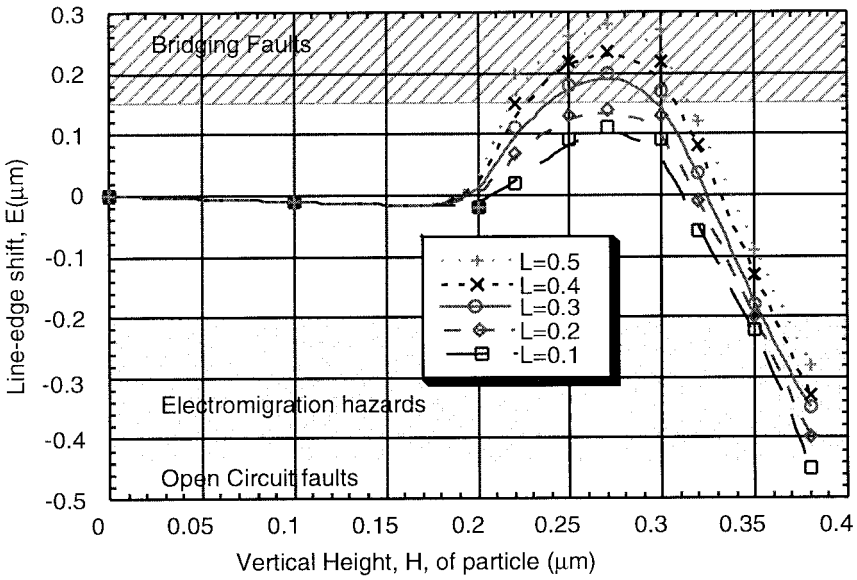

Fig. 9. Graph of line-edge shift E versus height H of W particles at different widths L.

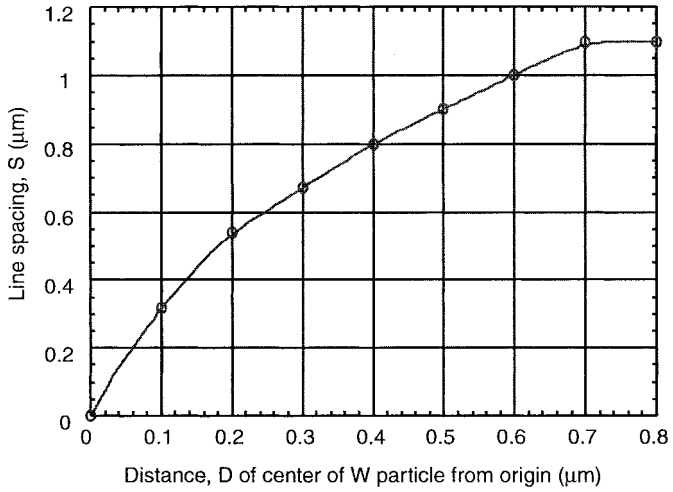

Fig. 10. Graph of line spacing S versus distance of center of tungsten particle from the origin.

occurs is at the origin and as the particle moves away from the origin the line spacing increases to the nominal value of 1.1 μm. The line spacing, S, for $0 < D < 0.8$ μm can be simply modeled as

$$S = 2.55D - 1.54D^2. \tag{4}$$

B. Nitride Defect Study

The next defect that we have modeled is a nitride defect. It was detected by the KLA 2132 following silicon nitride etch. The SEM image shows the effects of this defect, namely line-edge shifting and bridging (see Fig. 11). The structure simulated in METROPOLE is similar to the one shown in Fig. 12(a). Following nitride deposition on the wafer surface, the structure is covered by photoresist. Exposure and development of the photoresist followed by nitride etch in the ideal case defines nitride lines of width 0.4 μm and a line spacing, S, of 0.6 μm. Fig. 12(b) shows the benchmark simulation following photoresist development and etch.

When a nitride particle (width 0.4 μm and height 0.9 μm) is introduced on the silicon nitride surface, the photoresist is no longer planar but has a bump in the region over the nitride particle as seen in Fig. 12(a). The subsequent exposure of the photoresist to randomly polarized i-line illumination and subsequent development leads to an extra pattern as seen in the simulation results in Fig. 13(a). After the nitride etch and removal of photoresist, the extra pattern results in bridging between the nitride lines and this is illustrated in Fig. 13(b). Additionally, simulation results also indicate that nitride line-edge E2 also shifts in the direction toward the particle. This is possibly caused by the light scattering of the nonplanar photoresist surface toward line-edge E2 causing line-edge E2 to shift toward the particle. The SEM image in Fig. 11 shows a similar phenomenon of bridging between the nitride lines and line-edge shifts validating the simulator accuracy. The SEM images in Fig. 11 also show that the defect adheres to the surface. As a result, the defect propagates through the process and causes topography changes at later levels in the process flow.

To assess the effects of particle height and width on line spacing S, numerous simulations were performed. In a majority of cases, it was observed that the presence of nitride particle caused bridging. Moreover, it was found that the line spacing was between zero (bridging) and the nominal value of 0.6 μm. This indicates that there was no overetching of nitride lines and in all cases nitride line-edges move toward the particle. The region where bridging occurs was caused by different heights and widths of nitride particles was determined as the shaded region in Fig. 14. It can be seen that as the width of the particle increases, smaller height nitride particles are sufficient to cause bridging faults. Nitride line-edge E2 shifts were also studied using the same simulation results. The simulation results indicated that nitride line-edge E2 also shifts toward the particle. The extent of nitride line-edge E2 shift was however considerably less than in the case of nitride line-

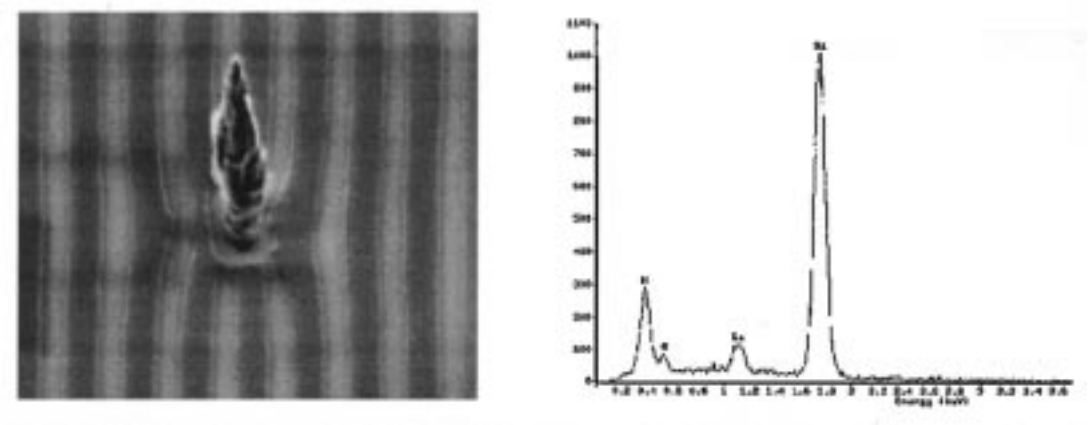

(a) (b)

Fig. 11. (a) The SEM picture of a particle and (b) an EDS study indicates the particle is a nitride particle.

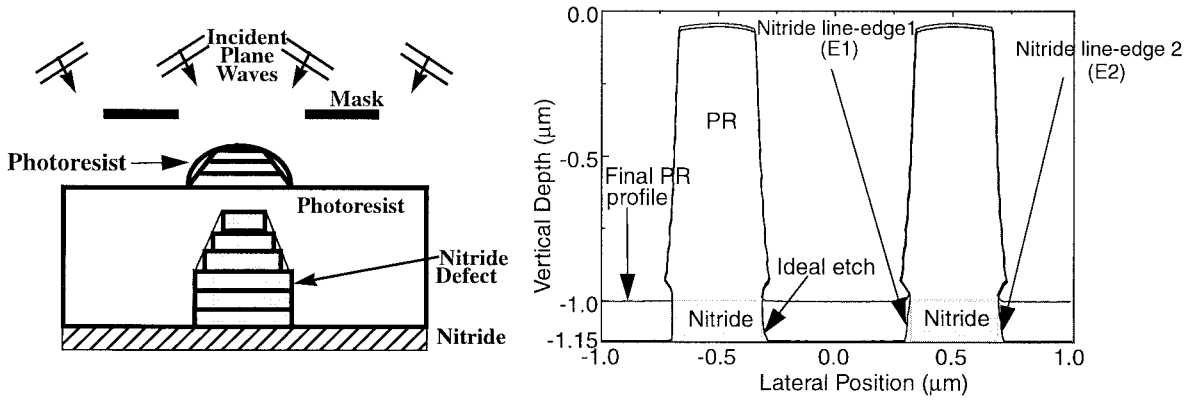

(a) (b)

Fig. 12. (a) Wafer structure for simulation and (b) simulation of ideal case after PR exposure and development and after nitride etching.

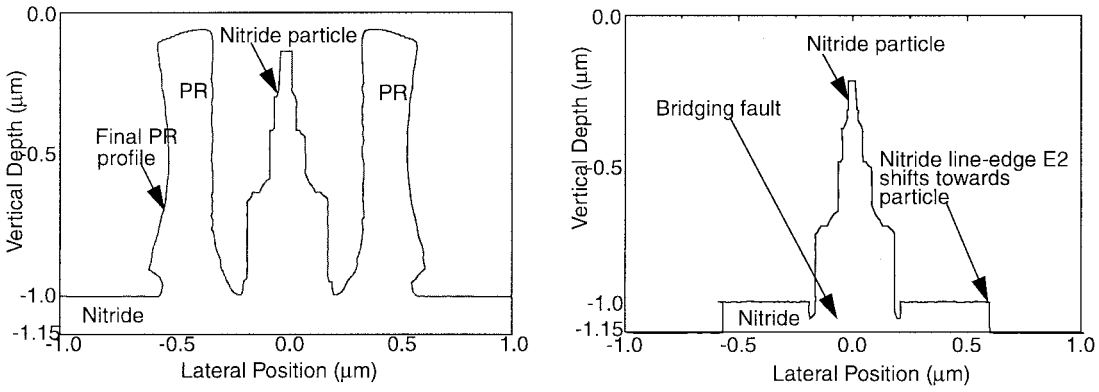

(a) (b)

Fig. 13. (a) Surface profile after PR development and exposure and (b) surface profile after nitride etch and PR removal.

edge E1. This is because nitride line-edge E1 is closer to the particle than nitride line-edge E2, therefore causing the particle to reflect more light toward line-edge E1.

The location of nitride particle was also investigated with respect to the line spacing. As the nitride particle of vertical height 0.9 μm and width 0.4 μm moves away from nitride line-edge E1, a relationship between the line spacing S and distance of the center of the particle from the origin (particle is symmetrical with respect to the mask) was obtained as shown in Fig. 15. It is seen that as the particle moves away from the origin, the line spacing increases steadily from 0 to the maximum nominal value of 0.6 μm. The line spacing S in Fig. 15 can be simply modeled as

$$S = \begin{cases} 0, & 0 \le D \le 0.1 \\ -0.24 + 2.66D - 1.96D^2, & 0.1 < D \le 0.5 \\ 0.6, & 0.5 < D \le 0.6. \end{cases} \quad (5)$$

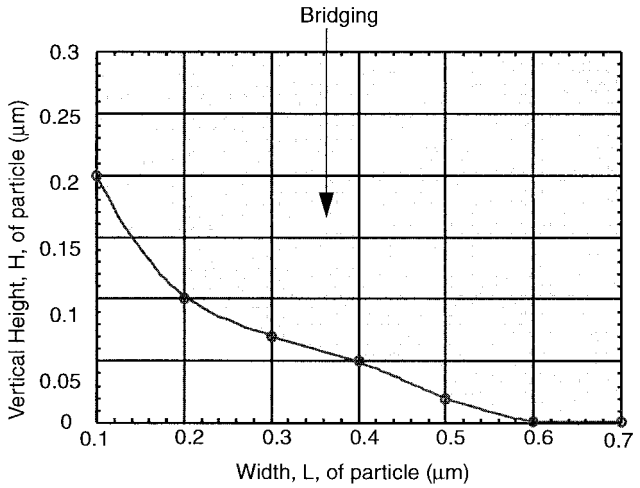

Fig. 14. Graph showing region of bridging.

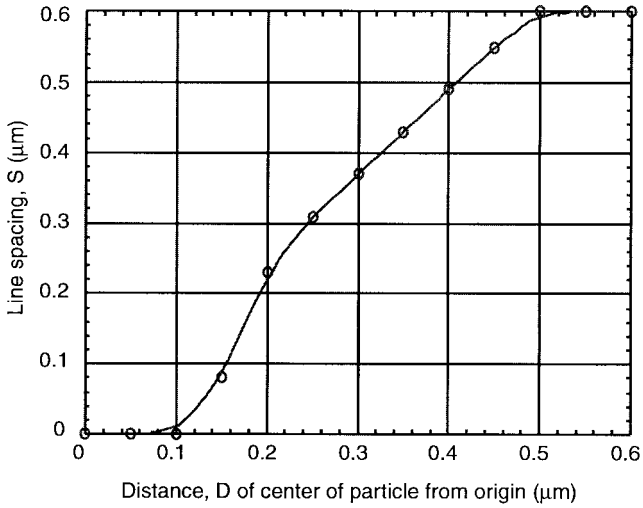

Fig. 15. Graph of line spacing S versus distance D of center of nitride particle from origin.

IV. Summary

A new methodology was described for development of macromodels for defects that propagate from one process step to another and have a significant impact on yield. The methodology involves measurements and analysis of in-line fab data, design of experiments using the rigorous topography simulator, METROPOLE, and finally the extraction of results from the experiments in the form of RSM-type macromodels. The macromodels developed are a function of such particle attributes as size, location, and chemical composition. This methodology is easily applicable to different devices and technologies. This will allow the determination of the sampling plan at each mask level and the choice of the most appropriate inspection sensitivity (pixel size) to capture the killer defects.

References

[1] R. K. Nurani, R. Akella, A. J. Strojwas, R. Wallace, M. McIntyre, J. Shields, and I. Emami, "Development of an optimal sampling strategy for wafer inspection," *ISSM*, pp. 143–146, 1994.

[2] R. K. Nurani, A. J. Strojwas, and W. Shindo, "Effects of defect propagation/growth on in-line defect based yield prediction," in *Proc. 2nd Intl. Workshop on Statistical Metrology*, 1997, pp. 44–47.

[3] X. Li, A. Strojwas, A. Swecker, M. Reddy, L. Milor, and Y. T. Lin, "Modeling of defect propagation/growth for yield impact prediction in VLSI manufacturing," *Proc. SPIE Microelectron. Manufact.*, Oct. 1997, pp. 167–178.

[4] X. Li, A. Strojwas, M. Reddy, L. Milor, and Y. T. Lin, "Modeling of defect propagation/growth for early yield impact prediction in VLSI fabrication," in *Proc. ASMC'97*, Boston, MA, Sept. 1997, pp. 263–268.

[5] M. Reddy, "Modeling of contamination to defect transformation for yield impact prediction in VLSI manufacturing," M.S. thesis, Dept. Elect. Comput. Eng., Carnegie Mellon Univ., Pittsburgh, PA, Sept. 1996.

[6] C.-M. Yuan, "Modeling of optical alignment and metrology in VLSI manufacturing," Ph.D. dissertation, Carnegie Mellon Univ., Pittsburgh, PA, 1989.

[7] K. D. Lucas, "Vector modeling of photolithography for VLSI semiconductor manufacturing," Ph.D. dissertation, Carnegie Mellon Univ., Pittsburgh, PA, 1995.

[8] C. E. Novak, K. D. Lucas, A. J. Strojwas, and Z. M. Lin, "Lithography simulation of contamination-caused defects," in *Proc. SPIE Int. Symp. Microlithography*, Feb. 1995.

[9] H. T. Heineken and W. Maly, "Manufacturability analysis environment—MAPEX," in *Proc. 1994 Custom Integrated Circuits Conf.*, May 1994, pp. 309–312.

[10] J. Khare, "Contamination-defect-fault relationship: Modeling and simulation," Ph.D. dissertation, Carnegie Mellon Univ., Pittsburgh, PA, 1995.

Xiaolei Li received the B.S. degree in semiconductor physics from Fudan University, Shanghai, China, in 1990, the M.S. degree in electrical engineering from the University of North Carolina, Charlotte, in 1993, and the Ph.D. degree in electrical and computer engineering from Carnegie Mellon University, Pittsburgh, PA, in 1997. His Ph.D. dissertation was on "rigorous topography simulation for VLSI manufacturing" in which he developed a physically based 3-D photolithography simulator and applied the simulation methods to yield improvement efforts.

He has had research experience in the area of defect formation during ion implantation and rapid thermal processing, silicon quantum diode structures, processing and material properties of III–VI compound semiconductor. He was working at AMD, Sunnyvale, CA, as a Visiting Engineer on defect growth/propagation project during the summer of 1996. He has over 20 publications in professional journals and conference proceedings. He has been with PDF Solutions, San Jose, CA, since November 1997 as a Senior Consulting Engineer. His current research interests include yield diagnosis and enhancement methodologies, process simulations, and advance device structures.

Dr. Li received a Best Paper Award in SRC Techcon'96 held in Phoenix, AZ.

Andrzej J. Strojwas (F'90) received the Ph.D. degree in electrical engineering from Carnegie Mellon University, Pittsburgh, PA, in 1982.

He is Professor of Electrical and Computer Engineering at Carnegie Mellon University and Co-Director of Pennsylvania SEMATECH Center of Excellence. He has held positions at Harris Semiconductor Co., AT&T Bell Laboratories, Texas Instruments, NEC, Hitachi, and SEMATECH. He serves as Consultant to a number of semiconductor companies in the area of statistically based CAD/CIM of VLSI circuits. His research interests include modeling of IC equipment, fabrication processes and semiconductor devices, computer-aided design and verification of VLSI circuits, and control and diagnosis of the IC fabrication processes.

Dr. Strojwas received the 1991 Best Paper Award from IEEE Transactions on Semiconductor Manufacturing.

Mahesh Reddy received the B.S. and M.S. degrees in electrical and computer engineering from Carnegie Mellon University, Pittsburgh, PA, in 1994 and 1996, respectively.

He is currently the Applications Engineer for KLA-Tencor, Dallas, TX, directing Texas Instrument's in-line monitoring use of defect inspection tools. In the past two years he has been working in yield engagement activities and automatic defect classification technology for KLA-Tencor at Texas Instruments DMOS5 and AMOS.

Linda S. Milor (S'86–M'90) received the Ph.D. degree in electrical engineering from the University of California, Berkeley, in 1992.

She is currently the Device Engineering Manager in the Yield Department in the Submicron Development Center, Advance Micro Devices (AMD), Sunnyvale, CA, where she has been since 1995. Before joining AMD, she was an Assistant Professor with the Electrical Engineering Department, University of Maryland, College Park. She has published in the areas of yield modeling, yield enhancement, circuit performance prediction, testing of analog integrated circuits, and statistical modeling.